

Published in final edited form as:

Crit Rev Biomed Eng. 2011 ; 39(4): 319–336.

Computational Modeling of Airway and Pulmonary Vascular Structure and Function: Development of a “Lung Physiome”

M. H. Tawhai^{a,*}, A. R. Clark^a, G. M. Donovan^b, and K. S. Burrowes^c

^aAuckland Bioengineering Institute, The University of Auckland, Auckland, New Zealand

^bDepartment of Mathematics, The University of Auckland, Auckland, New Zealand ^cOxford University Computing Laboratory, University of Oxford, Oxford, United Kingdom

Abstract

Computational models of lung structure and function necessarily span multiple spatial and temporal scales, i.e., dynamic molecular interactions give rise to whole organ function, and the link between these scales cannot be fully understood if only molecular or organ-level function is considered. Here, we review progress in constructing multiscale finite element models of lung structure and function that are aimed at providing a computational framework for bridging the spatial scales from molecular to whole organ. These include structural models of the intact lung, embedded models of the pulmonary airways that couple to model lung tissue, and models of the pulmonary vasculature that account for distinct structural differences at the extra- and intra-acinar levels. Biophysically based functional models for tissue deformation, pulmonary blood flow, and airway bronchoconstriction are also described. The development of these advanced multiscale models has led to a better understanding of complex physiological mechanisms that govern regional lung perfusion and emergent heterogeneity during bronchoconstriction.

Keywords

multiscale; respiratory; bronchoconstriction; perfusion

I. INTRODUCTION

Conceptual and mathematical models have been used extensively in pulmonary physiology. For example, the conceptual model of the lung as a “Slinky” serves to explain the deformation of the lung tissue under gravity, and more recently to explain some of the gravitational contribution to the development of a gradient in blood flow.¹ Mathematical models have been used to encapsulate a current state of knowledge, to develop hypotheses, and to guide experiments. Models that have led to new insights have not necessarily linked structure with function, although the link is usually implied. For example, West’s classic “zonal” model² relates pulmonary capillary perfusion to the local blood and alveolar air pressures. The blood pressures depend on hydrostatic pressure, which relates to the location of the capillary in the lung, hence implying a structural connection without explicitly including one. A further example is the estimation of gas exchange in the presence of a nonuniform distribution of ventilation (V) to perfusion (Q) ratios.³ By assuming that the lung consists of discrete units that each have a unique V/Q ratio, the integrative effect on

whole-lung gas exchange can be estimated. While these types of conceptual and quantitative modeling approaches have given important insights into the function of the lung, without an explicit link to the lung's structure and coupling to another function that occurs simultaneously and over multiple spatial scales, they are limited in their explorative or predictive ability with respect to the function of the intact *in vivo* organ. With the advent of modern medical imaging and the explosion in computing power, it is now possible to derive models that replicate the important geometric features of individual lungs, and to simulate function within these geometric models.⁴⁻¹⁰ This review describes a systematic effort by our group and others to develop such models within the framework of the Physiome and Virtual Physiological Human projects.¹¹⁻¹⁴ We will review some of the developments in an international collaborative effort to develop an integrative model of lung structure and function that spans multiple spatial scales, i.e., a so-called "multiscale" model. The models that will be described here consider scale-specific anatomical structure, and the emergence of behavior when force balance is integrated over multiple spatial scales.

The need for a quantitative understanding of *in vivo* lung function leads to the need for reliable model representation of the *in vivo* lung structure. The lung primarily comprises parenchymal (gas exchange) tissue, airways, arteries, and veins. The treelike structures of the airways and blood vessels are intimately bound to—and suspended within—the parenchyma (alveolar tissue). Symmetric,¹⁵ regular asymmetric,¹⁶ and fractal^{17,18} models of the airways and blood vessels have been used widely in modeling studies (e.g., Refs. 17–22, to name but a few). However, function in the lung is strongly influenced by the spatial positioning of the airways and vessels, and these convenient model simplifications do not provide such information. For example, ventilation distribution in the healthy lung is largely determined by peripheral tissue compliance (with a minor contribution from airway resistance in the normal adult lung), and effective tissue compliance depends on the gravitational deformation of the tissue, which varies regionally, and hence the connectivity between the airways and the tissue is essential for a model that predicts physiologically relevant ventilation distribution. A further example is illustrated in the West zonal model,² where the hydrostatic pressure gradient is a major determinant of the blood pressures at the capillary level, and this depends on location within the lung. Furthermore, recent studies have indicated that this is also dependent on vascular path length, which is heterogeneous and determined by the shape of the lung cavity.^{4,23}

Models of pulmonary function necessarily span multiple spatial and temporal scales (multiscale models). Dynamic molecular interactions give rise to whole-organ function, and the link between these scales cannot be fully understood if only molecular or organ-level function is considered. An appropriate multiscale model will capture the important features of function at each spatial or temporal scale while maintaining as much computational simplicity as possible. Physical forces acting on the surface of the intact lung are transmitted to the level of the gas exchange tissue (where they hold open the small airways and blood vessels) and on down to the level of cells and molecules where stress modulates local function.²⁴ The immediate response of the pulmonary airways to antagonists (such as allergens) generally occurs at the cellular level. However, this response results in emergent behavior at the scale of the whole lung via stimulation of smooth muscle cells in the airway walls. Similarly, mechanical obstruction of pulmonary blood vessels induces cellular-level response by direct interaction between an obstructing blood clot and the endothelium, and/or via local disruptions to pulmonary blood flow altering the local artery wall shear stress and activating release of nitric oxide (a potent vasodilator).²⁵ These cellular-level events ultimately lead to changes in whole-lung behavior. Surfactant secretion by type II alveolar epithelial cells in response to lung tissue stretch is a further classic example of multiscale interactions that determine global lung mechanics.²⁴

Here, we review progress in constructing appropriate multiscale finite element models of lung function. These include structural models of the whole lung and the pulmonary airways and vasculature, as well as functional models describing tissue deformation, pulmonary blood flow, and airway bronchoconstriction. These models differ from the class of models that are derived within the framework of a single hypothesis; because the models are—where possible—anatomically structured and their function is biophysically based, they can be transferred between different theoretical studies.

II. ANATOMICALLY STRUCTURED MODELS

Geometric model simplifications such as the reduction of the complex airway or pulmonary vascular trees to symmetric, regular asymmetric models or even lumped-parameter models have served—and will continue to serve—an extremely important role. However, heterogeneity in pulmonary structure and function is captured most accurately in anatomically structured models. This is of particular importance in studying localized disruption to pulmonary function, whether it is a response to agonist (e.g., asthma), a loss of parenchymal tissue (e.g., emphysema), or a blockage to an airway or blood vessel (e.g., pulmonary embolism).

A. The Lung

Finite element models of the lungs have been used in various applications, namely, as virtual phantoms to improve imaging protocols and image segmentation,²⁶ in predictive studies of tissue deformation for lung tumor tracking during radiation oncology,^{27–29} for studying the effect of gravity on tissue deformation,^{10,30–32} and as a tethering tissue in which model airways and vessels are embedded.^{5,33} Creating an anatomically structured finite element model of the lungs and/or lobes is typically achieved in one of two ways: (i) using commercially available software to convert volumetric imaging into a triangulated mesh of the organ surface, and then filling the volume that is bounded by the surface with a (usually tetrahedral) volume mesh. or (ii) warping a generic structured model to fit the surface shape of volumetric imaging (“geometry fitting”).^{34,35} The first method is the most widely used, and is also the typical method employed for generating meshes of airway or vascular trees for computational fluid dynamics (CFD) analysis. Because biological structures are usually curvilinear, using linear elements results in the necessity for highly discretized meshes. In addition, linear elements suffer from discontinuous derivatives at element boundaries. In tissue mechanics problems where stress is a function of the derivative of mesh displacement, this discontinuity can cause solution errors. On the other hand, nonlinear elements can (but do not always) allow for derivative continuity at element boundaries. One example of a nonlinear interpolation (or basis) function that provides continuity of the derivative between elements is cubic Hermite interpolation. Along with as the lung, cubic Hermite meshes have been used to describe the geometry of the torso,³⁴ the patella,³⁶ and several other organs.

B. The Airways

CFD has relatively recently become a viable method for numerically studying patterns of flow, pressure, and resulting particle transport in the airways. Prior studies have suggested that an anatomically accurate geometry is essential for a thorough understanding of airway flow.^{37,38} Medical imaging (typically CT, computed tomography) is now used routinely to construct geometric models of the upper-to-central airway. Recognizing the importance of anatomical geometry in the prediction of airflow, several groups have constructed models based on *in vivo* volumetric imaging,^{8,39–42} and 3D CFD is beginning to be used to understand intersubject variability in inhaled fluid transport,⁴³ and response to clinical interventions.⁴⁴ A limitation of 3D CFD is that it is usually restricted to analysis of relatively small portions of the airway (or vascular) tree. 3D CFD requires substantial

computing resources; simulations cannot be performed rapidly, and they require substantial postprocessing. In contrast, 1D models give a less accurate prediction of pressure drop, and only provide local mean airflow, but models can be solved rapidly within a 1D geometry, and so this methodology allows inclusion of the entire airway tree. The 1D model is also more amenable to coupling with other functional models at higher or lower spatial scales, e.g., soft tissue mechanics⁷ or cellular function.⁴⁵

1. Image-Based Airways in 1D—Two methods have been proposed for modeling the 3D spatial distribution of the airway tree. Kitaoka et al.⁴⁶ presented a method to generate a branching structure that was bounded by a curvilinear surface, where the length of the generated airways was proportional to branch diameter, the diameter in turn was proportional to flow, and flow was determined by the branch's location within the tree. The fundamental basis of the method is therefore Murray's law, $d_p^x = d_1^x + d_2^x$, i.e., that parent branch diameter d_p raised to the power of x is the sum of each child branch diameter (d_1 and d_2) to the power of x ,⁴⁷ where x is a constant that holds throughout the airway tree. Additional rules were required in the algorithm to give the branches direction (branching and rotation angles), and to ensure that airways remained within the bounding lung surface. The Kitaoka model demonstrated that basic hypotheses for lung structure and function (diameter proportionality and Murray's law) could be consistent with the complexity of the human airway tree. The authors found it challenging, however, to maintain exact consistency with Murray's law and at the same time satisfy the geometric constraint of the tree remaining within the lung-shaped volume. The Kitaoka model has been used in subsequent functional modeling studies.⁴⁸ However, because it is a generic model, it has not been used for studies that require subject-specific airway geometry.

Tawhai et al.^{33,49} proposed a different method that extended the 2D algorithms of Wang et al.⁵⁰ and Nelson and Manchester⁵¹ to the 3D lung. In this method, the distribution of airways is generated on the basis of "supply and demand," and the airway diameters are added as a postprocessing step. For a set of volumetric images (from human or animal) attained at total lung capacity (TLC), a volumetric finite element mesh is first geometrically fitted to the lobes/lungs as outlined in the previous section. The volume mesh is then filled with a grid of uniformly spaced points, each point representing the location of a pulmonary acinus. The acinus grid is uniformly spaced under the assumption that the lung tissue is close to uniformly expanded at TLC. This is a reasonable approximation for the upright lung, where maximal expansion can be attained, but is much less likely in the supine lung (the usual imaged posture) due to shifting abdominal contents restricting the caudal displacement of the diaphragm. The assumption of uniformly expanded tissue at supine TLC therefore introduces error in the method. Whether this has a significant effect on the geometry of the generated tree is unclear. An initial 1D finite element mesh placed along the centerlines of the segmented airways acts as an initial condition for the algorithm. New branches are generated from the ends of the previous generation by directing a branch toward the center of mass of a subset of the acinus grid points, where points in any current subset are those that are closest to the parent branch. This continues recursively until each acinus grid point is supplied by a single terminal model airway. A 1D airway model generated for a single subject is illustrated in Fig. 1A.

The Tawhai method generates tree models that are subject specific with respect to the geometry of the largest (segmented) airways and the shape constraint on the tree of the subject's lungs and/or lobes. The algorithmically generated airways cannot exactly match the individual's airway tree, however, the averaged geometric characteristics of the model are consistent with measured human airway morphometry.^{15,52–54} The method has also been shown to be appropriate for generating the more asymmetric airway geometry of the ovine lung.³³

Because the anatomically structured model is generated within a volumetric finite element model for the lung, it inherently has connectivity to the model tissue, i.e., as the lung model deforms, the airways deform with it. This is an advantage for coupling airway and lung tissue function, as will be described in subsequent sections.

2. 3D-1D Image-Based Airway Models—To study airflow as it evolves over the full range of spatial scales in the lung, from the turbulent flows in the mouth or nasopharynx to the low-Reynolds number flows in the alveolar tissue, remains a considerable challenge. Lin et al.⁴² presented a method for creating subject-specific airway mesh geometries that incorporate the desired level of 3D or 1D geometric detail wherever it is required in the airway tree, with seamless transition between the 3D and 1D scales. The method is summarized in Fig. 1. In this approach, 1D models for the entire conducting airway tree³³ are converted to a cubic Hermite surface mesh with smooth and continuous surfaces at the bifurcations (Fig. 1B), and this is combined with the geometrically fitted surfaces of a model for the uppermost (image-based) airways. Any portion of this model can be selected for 3D (tetrahedral or structured) meshing for its application in CFD analysis (Figs. 1C and 1D). A convenience of the approach is that the lower order airways remain in the model (Fig. 1E), providing a direct connectivity to the deforming lung tissue (by coupling to tissue mechanics,¹⁰ or to deformation defined by image registration⁵⁵). This removes the need to prescribe assumed or artificial boundary conditions at the model periphery.

C. Pulmonary Vasculature

Constructing anatomically based functional models of the pulmonary vasculature that are representative of the important structural features of the pulmonary circulation while remaining computationally tractable is a considerable task. Each of the bronchial airways of the human lung is “accompanied” by an arterial vessel, but there are many more pulmonary arteries than there are branches in the bronchial airway tree,⁵⁶ and the same is true for the venous system. These additional blood vessels have been termed “supernumerary” vessels. The bifurcating system of accompanying and supernumerary vessels extends to the level of the pulmonary capillaries, transporting blood to the gas exchange surface. Within the pulmonary acini, which are generally defined to be the functional gas exchange units of the lung, small arteries, and veins are connected by capillary sheets that cover the alveoli arising at multiple levels throughout the structure. The extra-acinar and intra-acinar vessels therefore have distinct geometric structures that give rise to scale-specific function, i.e., the preacinar vessels of the human lung branch dichotomously (with the exception of the supernumerary vessels described below) and hence supply blood to the gas exchange units in a parallel arrangement, and the intra-acinar vascular structure results in combined series and parallel perfusion. Approaches to modeling the distinct geometry and characteristics of blood flow within these regions are considered here.

1. Arteries and Veins—The methods described previously for developing anatomically based models of the pulmonary airways are directly applicable to the development of models of the accompanying pulmonary arteries and veins. A departure from the branching geometry of the airways—and a further complexity to be considered in model development—is the presence of supernumerary vessels, which do not match a corresponding bronchial airway. While their function has been studied in isolated *ex vivo* studies, e.g., by Bunton et al.,⁵⁷ their function in the intact lung is currently poorly understood and their functional significance is unknown. Since supernumerary vessels are not visible on angiograms, it has been suggested that they are not perfused under normal conditions,⁵⁶ but the functional role of these vessels may become important during perturbations in the circulatory demand or supply. The only mathematical model to date that has explicitly included a description of supernumerary vessels is that of Burrowes et al.⁵ However, in this model, all

supernumeraries were assumed to be either fully perfused or not perfused at all. Other models either exclude supernumerary vessels completely (e.g., symmetric dichotomous trees) or have included them implicitly (in the same way as conventional vessels) as defined from morphometric measurements.

Burrowes et al.⁵ constructed geometric models of the pulmonary arterial and venous trees—including supernumerary vessels—by segmenting the largest arteries and veins from MDCT data and using the volume-filling algorithm, described previously, to construct accompanying blood vessels to the level of the terminal bronchioles (all extra-acinar blood vessels). Supernumerary vessels were constructed in a postprocessing step via an algorithm designed to mimic the (relatively limited) known geometric characteristics of supernumerary vessels. That is, assuming that supernumerary vessels emerge at a branching angle close to 90 deg from the accompanying branch, and bifurcate rapidly to supply the closest parenchymal tissue. As with the pulmonary airways, blood vessels were represented by 1D finite elements distributed in 3D space within the lung volume. Fig. 2 illustrates the steps in this process.

2. Intra-Acinar Arterioles, Venules, and Capillaries (the “Ladder” Model)—To maintain computational tractability in models of the whole lung that explicitly describe each extra-acinar blood vessel, a lumped-parameter (or averaged) description of the acinus is necessary. However, to first understand intra-acinar function, it is necessary for models to “zoom in” on the complex structure of the acinus and to model aspects of this structure—and pulmonary function within it—explicitly. The airways and air spaces in the acinus branch in an irregular dichotomy with an average of nine generations (range 6–12).⁵⁸ There have been several modeling attempts to capture this structure, both using an abstract “fractal” approach⁵⁹ and via anatomically based representations of the acinus that statistically match morphometric measurements.^{60,61} However, models of perfusion within the pulmonary acinus have not followed the development of the airway models.

Intra-acinar arterioles and venules are high-resistance vessels that branch along and between the alveolated airways, and have numerous small (precapillary) vessels arising from their walls. These vessels lead to the capillary units that cover the alveolar septae.^{62,63} Capillaries, on the other hand, have no apparent regular branching structure in the lung, and are so dense that they are often considered to form a “sheet.”⁶⁴ Despite this complex acinar structure, models of perfusion and gas exchange that include acinar blood vessels have typically represented the whole acinus as a single continuous capillary bed in terms of branching structure and governing physical equations.^{19,65,66} In these models, arteries and veins are coupled only at their most distal location by a single microcirculatory unit, effectively assuming that perfusion is equal everywhere within an acinus.

Recently, Clark et al.⁶⁷ developed a geometric description of the acinar blood vessels that distinguishes between small noncapillary (arterioles and venules) and capillary vessels. Arterioles and venules are represented as distinct elastic vessels following the branching structure of the acinar airways. These vessels are assumed to be joined at each generation by capillary sheets that cover the alveoli present at that generation, forming a ladderlike structure, as shown in Fig. 3. Because the model accounted for both serial and parallel perfusion pathways, it was able to reproduce the decrease in blood flow rates in the distal part of the acinus compared with the proximal part that had previously been observed in animal studies.^{68,69} This is something that was not possible using previous models of the pulmonary circulation. When the ladderlike model was connected to a symmetric extra-acinar vascular structure, a decreased pulmonary vascular resistance (PVR) was observed when compared with a model in which each acinus was represented by only a single continuous capillary sheet (parallel perfusion alone).

The ladderlike acinus model still includes a geometrical simplification of the capillary bed, namely, Fung's sheet flow description.^{64,67} This approximates the dense pulmonary capillary bed as a sheet of fluid flowing around posts of connective tissue, and bounded by the compliant capillary wall. This model provides a computationally efficient prediction of average blood flow and cellular transit times through an alveolar septum. To model perfusion in the capillary bed at an even finer spatial scale, Burrowes et al.⁷⁰ explicitly described the capillaries that extend over an alveolar sac (19 adjoined alveoli) as tubules. This model was based on previous studies that covered smaller portions of the capillary network,^{71,72} and was able to describe perfusion heterogeneity in the smallest pulmonary vessels as it related to the geometric constraints of the alveolo-capillary structure and the spacing of the supplying arterioles and draining venules.

III. COMPUTATIONAL MODELS OF PULMONARY STRUCTURE AND FUNCTION THAT SPAN MULTIPLE SPATIAL SCALES

This section considers two examples of the development of multiscale models for studying airway and vascular function. The aim is to demonstrate models that span from cellular to whole-organ function, and explain the new insights that such models can provide. But before the multiscale models are introduced, we review some recent efforts in modeling the mechanics of the intact lung. This is considered first because the lung's tissue deformation is an "organ-level" event that has consequence for both of the modeling examples that will be presented.

A. Soft Tissue Mechanics of the Intact Lung

Early conceptual and computational models of lung deformation mechanics were developed to demonstrate that ventilation distributes nonuniformly in the lung,⁷³ and that the lung deforms under its own weight.³² Models such as these, and the experimental studies that led to and followed their development, established the fundamental principles of respiratory biomechanics. Further finite element studies followed, for example, directed at understanding the effect of heart weight on lung tissue deformation.³⁰ The finite element model geometries were idealized, for example, employing axisymmetry to reduce the model complexity,³² and usually used linear elastic moduli (constant, or pressure dependent^{30,32}), or occasionally a relatively simple nonlinear strain energy density function.¹⁰ These simplifications have been necessary because modeling of lung tissue deformation is confounded by two main challenges, namely, access to sufficient computing power, and an accurate constitutive law to relate stress and strain in the lung tissue. The first challenge has been overcome, but the second remains. Linear elastic moduli for the lung tissue can be attained through indentation testing,⁷⁴⁻⁷⁶ and nonlinear moduli through fitting to data from stretching of excised tissue strips. Each approach has limitations, i.e., for a constant rate and volume of breathing (i.e., when viscoelastic effects can be neglected), the lung tissue behaves as nonlinearly pseudo elastic, hence the linear moduli only provide an approximation at discrete inflation pressures, and tissue strip specimens distort the *in vivo* alveolar geometry and do not include the normal surface forces that are so important for determining the integrated elasticity of the lung. That the lung tissue is in fact viscoelastic becomes important when considering expansion and recoil of the lung at different rates and/or volumes. This is particularly important to enable bridging between continuum models and models for oscillation mechanics, where tissue viscoelasticity is an essential property of the oscillating system.⁷⁷

Despite the lack of a precise definition for the stress-strain relationship of the lung tissue, finite element models of the lung have recently shown potential for predicting lung motion for radiation therapy planning.^{27-29,78} Lung motion confounds the localization of radiation

to the lung tumor in that otherwise healthy tissue is also irradiated, causing acute and chronic changes in the tissue structure that adversely affects gas exchange function. The goal of these modeling studies is to develop a clinically applicable tool that can predict subject-specific breathing motion and regional tissue displacement during therapy in order to improve treatment planning and efficacy. Because the treatment is given in a single posture (supine), it is a sufficient approximation to use 4D-CT (“four-dimensional” computed tomography) to capture tissue motion over one or several breaths. Some studies use image registration between adjacent time points in the breathing cycle to estimate localized linear elastic moduli to represent the relationship between stress and strain in the tissue, others treat the lung tissue as isotropic and homogeneous, and use a nonlinear strain energy density function rather than fitted distributed values. The latter method has been demonstrated to give reasonable predictions of tissue and tumor displacement, which is surprising considering that patients with lung cancer are typically smokers with significantly non-normal tissue elasticity, and hence are likely to have greater heterogeneity of tissue elastic properties and tissue expansion than normals.

The assumption that the lung parenchyma is homogeneous and isotropic is more appropriate for the healthy lung, but even in this case it is a gross approximation. Again, surprisingly, this simple approach has been shown sufficient to predict tissue deformation due to gravity and the weight of the lung in the supine posture in multiple subjects. Tawhai et al.¹⁰ use finite deformation elasticity theory to predict tissue displacement, with strain energy density,

$$W(E)=C/2\exp(\alpha J_1^2+\beta J_2), \quad (1)$$

due to Fung,⁷⁹ where J_1 and J_2 are the first and second invariants of the Green strain tensor E . This relatively simple strain energy density function, when parameterized to the average expansion pressures considered typical at resting and maximal volumes for the human lung, predicts elastic behavior that is consistent with pressure-dependent bulk and shear moduli measured experimentally,⁷⁶ as shown in Fig. 4. The model is first expanded from a reference volume (at half of FRC, functional residual capacity) to FRC in the absence of gravity. Gravity is added in a second step, using frictionless contact constraints to maintain contact between the lung surface and a bounding “pleural” surface that remains rigid. The lung is free to slide against the pleural surface. This study considered two very different subjects, namely, a young healthy male with a relatively large lung, and a female with small airways disease who had a relatively small lung. The same coefficients for Eq. (1) were assumed for both subjects, and the model predicted distributions of tissue density that compared well with tissue density calculated directly from supine CT imaging of each subject. Results from this study are illustrated in Figs. 5 and 6, with Figs. 5A and 5B showing subject-specific predictions of tissue density distribution (mean \pm SD) compared with CT measurement, and Fig. 6 illustrating the prediction of a smaller pleural pressure gradient in the prone model than in the supine model. Since this study, the analysis has been repeated on \sim 30 subjects, and for the majority of subjects, the model prediction provides a good match to the subject’s CT measurement (unpublished findings).

A model deformation can be used to interact with embedded models of the airways or vessels. Interaction occurs via displacement and axial stretch of the embedded structures, and through the local tissue tethering pressure that acts on the airway or vessel wall. The tethering pressure for a vessel or airway that is being passively deformed (without vaso- or bronchoconstriction) can be approximated as the local elastic recoil pressure of the tissue. This interaction is considered in both of the following multiscale model examples.

B. Airway Bronchoconstriction

Airway bronchoconstriction is an area in which multiscale phenomena are thought to be important,⁸⁰ because there are many hypothesized biophysical mechanisms that span multiple spatial scales. Studying the relative importance and interactions between these phenomena is very difficult, if not impossible, by considering each scale only in isolation. Hence, the development of multiscale models is an important area of research. There are a number of models fitting this description to various degrees in the literature, such as the terminal airway unit model of Anafi and Wilson⁸¹ and its well-known Mandelbrot-tree implementation by Venegas et al.,²¹ the airway constriction model of Affonce and Lutchen,⁸² and the airway constriction and agonist binding model of Amin et al.⁸³ Here, we review the multiscale model of bronchoconstriction developed by Politi et al.,⁸⁴ since this model has been developed within the anatomically structured and biophysically based modeling framework that is the theme of this review.

Politi et al. present a multiscale, spatially distributed model of bronchoconstriction associated with asthmatic airway hyperresponsiveness, which couples models at four spatial scales. The scales considered are the molecular, wherein applied agonist triggers elevated intracellular calcium concentrations; the cellular, which incorporates sliding filament theory⁸⁵ to account for airway smooth muscle (ASM) contraction dynamics,⁸⁶ as induced by agonist and calcium; the tissue scale, which incorporates both airway wall mechanics and increases in parenchymal tethering due to airway constriction; and finally the organ level, where a continuum mechanics approach accounts for mechanical deformations due to breathing and gravity.

At the largest spatial scale, the organ level, the lung parenchyma is modeled as an initially isotropic 3D hyperelastic continuum using the approach of Tawhai et al.¹⁰ and Fung's material law,⁷⁹ as previously described. The computational domain may either be a patient-specific geometry acquired from CT imaging, or to make the model amenable to more mathematical analysis than is possible in the complex full tree, it can simply be a spatially restricted block of lung tissue representing a small portion of the lung. Gravity and breathing patterns are specified, and the resulting mechanical deformations and material states are found computationally by a finite element solution.

Embedded within this parenchymal continuum is the conducting airway tree, asymmetrically bifurcating and classified by Horsfield order.¹⁶ Each conducting airway is modeled as a right cylinder described only by its radius, and thus fundamentally 1D. This plane strain model incorporates three airway layers, i.e., an outer "local" parenchymal layer, connected with the global organ-level parenchyma and with material properties determined by that as described later; an airway smooth muscle layer; and an airway wall layer.

The local parenchymal layer is a linearization of the global parenchyma that accounts for an increase in tethering pressure due to airway constriction. The airway smooth muscle layer is incompressible, with ASM force determined by the smaller-scale models (details to follow). The pressure-radius relationship of the airway wall itself is described by the empirical relationship of Lambert et al.²⁰

Activation and force generation of the ASM is modeled by a Huxley-Hai-Murphy-style sliding filament model^{85,87} specifically modified to the unique properties of airway smooth muscle.⁸⁶ Changes in muscle length are represented by the relative movement of actin and myosin filaments, and force generation occurs via the cross-bridge cycle, wherein actin heads bind and unbind from binding sites on the myosin filament. There are four possible states in the model: unbound, unphosphorylated; unbound, phosphorylated; bound, phosphorylated; and bound, unphosphorylated. Only phosphorylated myosin can bind. Force

exerted by the ASM is determined by the number and position of bound sites. The rates of binding and unbinding are determined by agonist and calcium concentrations, which in turn are determined by molecular-scale modeling. At this smallest scale, dynamics of intracellular calcium determine the intracellular calcium concentration resulting from applied agonist.

Thus, an applied agonist triggers increased calcium, which in turn drives actin-myosin binding and thus ASM force generation. ASM force is opposed by parenchymal tethering and airway wall mechanics, and these forces must be balanced in order to determine the airway radius. This process is repeated for each airway at each time step. The multiscale interactions between all scales are summarized schematically in Fig. 7.

One complication is that the airway pressure-radius relationship can, in certain situations, be multivalued.^{20,82} That is, for a given value of muscle-generated force, it is in principle possible to have two (or more) different radii for which all forces are in balance. In a static model, “jumps” (that is, instantaneous transitions) between these solutions are possible. However, in this dynamic model, transition between states is modulated by ASM dynamics; infinite smooth muscle velocities, and thus jumps, are not possible. The result is slow and smooth transition in agreement with the experimental data.⁸⁸ The slow and smooth transition also contributes to solution stability.

One important result from this model is that even within a spatially restricted tissue unit ($10 \times 10 \times 20$ mm, 90 conducting airways), there is emergent spatial heterogeneity. For example, see Fig. 8 showing the spatial distributions of both tissue pressure (left panel) and airway radius (right panel) at the conclusion of a simulated agonist challenge.

While there are potentially important physiological features not yet included in the model (e.g., airflow pressures within the conducting airways themselves, passive ASM mechanical properties, surface tension and surfactant, etc.), the most intriguing possibility with this and similar models is the ability to examine the interactions between and relative influence of phenomena at multiple scales.

C. Pulmonary Circulation

Blood flows through successively smaller vessels in its passage through the pulmonary circuit. Travel begins through the pulmonary trunk, with a diameter of ~ 3 cm. Eventually blood is transported through the smallest (capillary) vessels, which range between approximately 1 and 15 μm in diameter (~ 8 μm on average).¹⁵ In the larger vessels, blood can readily be assumed to flow as a Newtonian fluid. However, at the microcirculatory level, particles suspended in blood—particularly red and white blood cells—strongly influence the apparent viscosity of blood and therefore the blood flow in each segment. At this level, the blood is no longer classed as a Newtonian fluid, and different flow models must be applied across the scale of vessels, thus introducing a multiscale nature to the problem of fluid mechanics within the pulmonary circuit. All of the vessels are embedded within the parenchymal tissue, introducing the “organ-scale” and a multiphysics problem.

Perfusion can be modeled in the 1D system described in Section II.C.1 by solving 1D Navier-Stokes, continuity, and vessel elasticity equations (as in Ref. 6), or if a steady state distribution is sufficient to give insight into the system function, by solving the Hagen-Poiseuille, continuity, and vessel elasticity equations.^{7,89} An important addition to this system of equations is a term that accounts for the weight of the blood, as a function of gravity, in the elastic vessels.

For a model of the pulmonary arteries, considered in isolation from a capillary bed and venous tree, boundary conditions must be specified at the pulmonary trunk (the “inlet”), at each artery “outlet,” and on each artery wall. The boundary condition at the inlet is a pressure or flow that is consistent with physiological values; the boundary condition on the arterial walls is the pressure exerted on the arteries by the surrounding tissue. The tissue pressure can be represented most simply by assuming that this is of equal value to the pleural pressure at the same isogravitational height. The boundary condition at the outlets must be assumed, and this is a significant limitation of any model that only considers flow in the arterial network.

In the earliest studies that simulated blood flow through anatomically based models of the entire accompanying arterial tree,^{4-7,89} these boundary conditions were necessary due to the computational difficulty in connecting each terminal artery and vein with an appropriately simplified representation of an acinar unit, which has a structure that is at least as complex as that of the extra-acinar blood vessels. These isolated artery models allowed investigation into the relative influence of gravity and structure on the distribution of pulmonary perfusion—a question that is hotly debated in the literature.⁹⁰⁻⁹² The model studies suggested that there is an underlying pattern of blood flow that can be attributed to the branching geometry of the vascular trees, and that the branching asymmetry contributes substantially to isogravitational heterogeneity of tissue perfusion. Both of these conclusions had previously been suggested on the basis of experimental studies,^{17,23} and the model provided additional evidence to support this. An example of the translation of this type of biophysically based and anatomically structured model from one study to another without the need to “redesign” was the same model’s application in an interspecies comparison of perfusion distribution.⁸⁹ Understanding interspecies differences (particularly between humans and typical experimental species) is important for appropriately interpreting animal studies in the context of human physiology. The Burrowes et al. study⁸⁹ demonstrated that the greater geometric asymmetry in the ovine arterial tree with respect to human is sufficient to cause significant differences in the regional distribution of blood flow, particularly in the gradient of blood flow in the gravitational axis.

These previous studies prescribed the boundary condition on the artery wall by assuming a linearly increasing pleural pressure as a function of the gravitational height within the lung. This does not take into account any variability of tethering pressures within an isogravitational plane, nor any shape change associated with tissue deformation due to gravity and breathing. Most recently, predictions of tissue deformation and elastic recoil pressure determined from the soft tissue mechanics model described in Section II.A.2 were used to define blood vessel dimensions in the perfusion model.⁷ This allowed more accurate comparison between postures and volumes than was previously possible. All of these previously described models suffered from the assumption of pressure boundary conditions at the terminal blood vessels. Pressures at this level of the pulmonary circulation are not readily measurable, and certainly not in the vast number that would be required for accurately prescribing boundary conditions in the distributed model. What is much more readily available are blood pressure and flow rates at the level of the heart (pulmonary artery and left atrium). Therefore, the next logical progression for the anatomically based models of the pulmonary vasculature described above is to connect the terminal arteries and veins with representations of the vasculature of the pulmonary acinus.

A model of the full pulmonary circulation (arteries, arterioles, capillaries, venules, veins) is made possible by the construction of appropriate models at each spatial scale, which can be combined to describe whole-organ perfusion.⁹³ First, the 1D, spatially distributed model of extra-acinar blood vessels described in Section II.C.1 provides a realistic picture of perfusion heterogeneity in the lung due to its asymmetric branching structure and variable

path lengths. Second, a symmetrically branching structure representing intra-acinar arterioles and venules connected at each level by capillary beds provides the stratified perfusion distribution in the acinus, which enables PVR to be low enough for the lungs to carry the whole cardiac output.⁶⁷ This structure is simplified in that it does not represent the asymmetry in arteriole and venule branching structure, but it allows a full-lung model to be solved numerically within a reasonable time. Third, a lumped-parameter model of capillary perfusion⁶⁴ is coupled with the explicit representations of larger vessels. This provides predictions of blood flow and red blood cell transit times on the level of 10 to 15 alveoli without the need to describe each and every capillary blood vessel. Finally, with the lung considered as a whole and its tissue approximated as a continuum, the soft tissue mechanics model described in Section II.A.2 provides a reasonable estimate of the deformation of blood vessels under gravity at different lung inflations.

Together, this coupled model spanning the scales of the whole-lung, individual vessels, acinar, and capillary units provides a valuable tool for studying the mechanisms that contribute to the regional distribution of perfusion. The model can demonstrate that each structural and gravitational feature of the pulmonary circulation makes a distinct contribution to the distribution of blood, i.e., postural differences in perfusion gradients can be explained by the combined effect of tissue deformation and extra-acinar blood vessel resistance to flow in the dependent tissue, hydrostatic effects play an important role in establishing an underlying gravitational perfusion gradient in the absence of tissue deformation, and coupling of large- and small-scale models reveals significant variation in microcirculatory driving pressures within isogravitational planes due to extra-acinar vessel resistance and amplification by the complex balance of pressures, distension, and flow at the microcirculatory level.

IV. CONCLUSIONS

Two examples of multiscale models that have been developed within the framework of the Physiome and VPH projects were reviewed here, and the advantages of considering function that emerges through the interaction of events at different spatial scales were considered. The principal challenges that remain for such modeling studies are to obtain experimental data that allows validation of each model component, and secondly to determine how these complex models can be reduced to a form that allows study of their behavior using established mathematical methods. The first of these issues is something of which most modelers are painfully aware. The second issue will become more important as we increasingly rely on numerical solutions to models, which are growing in complexity.

Acknowledgments

This work was supported by NIH Grants No. HL103405 and No. HL094315, and by NZ Health Research Council Grant No. 09-143.

References

1. Hopkins SR, Henderson AC, Levin DL, Yamada K, Arai T, Buxton RB, Prisk GK. Vertical gradients in regional lung density and perfusion in the supine human lung: the Slinky effect. *J Appl Physiol.* 2007; 103(1):240–8. [PubMed: 17395757]
2. West JB, Dollery CT, Naimark A. Distribution of blood flow in isolated lung; relation to vascular and alveolar pressures. *J Appl Physiol.* 1964; 19:713–24. [PubMed: 14195584]
3. Paiva M, Engel LA. Theoretical studies of gas mixing and ventilation distribution in the lung. *Physiol Rev.* 1987; 67(3):750–96. [PubMed: 3299409]

4. Burrowes KS, Hunter PJ, Tawhai MH. Investigation of the relative effects of vascular branching structure and gravity on pulmonary arterial blood flow heterogeneity via an image-based computational model. *Academic Radiol.* 2005; 12(11):1464–74.
5. Burrowes KS, Hunter PJ, Tawhai MH. Anatomically-based finite element models of the human pulmonary arterial and venous trees including supernumerary vessels. *J Appl Physiol.* 2005; 99:731–8. [PubMed: 15802366]
6. Burrowes KS, Tawhai MH. Computational predictions of pulmonary blood flow gradients: gravity versus structure. *Respir Physiol Neurobiol.* 2006; 154(3):515–23. [PubMed: 16386472]
7. Burrowes KS, Tawhai MH. Coupling of lung tissue tethering force to fluid dynamics in the pulmonary circulation. *Int J Numer Methods Biomed Eng.* 2010; 26:862–75.
8. Lin CL, Tawhai MH, McLennan G, Hoffman EA. Characteristics of the turbulent laryngeal jet and its effect on airflow in the human intra-thoracic airways. *Respir Physiology & Neurobiol.* 2007 Aug 1; 157(2–3):295–309.
9. Lin CL, Tawhai MH, McLennan G, Hoffman EA. Computational fluid dynamics: multiscale simulation of gas flow in subject-specific models of the human lung. *IEEE Eng Med Biol.* 2009; 28(3):25–33.
10. Tawhai MH, Nash MP, Lin CL, Hoffman EA. Supine and prone differences in regional lung density and pleural pressure gradients in the human lung with constant shape. *J Appl Physiol.* 2009 Sep; 107(3):912–20. [PubMed: 19589959]
11. Crampin EJ, Halstead M, Hunter PJ, Nielsen P, Noble D, Smith N, Tawhai MH. Computational Physiology and the Physiome Project. *Exp Physiol.* 2004; 89(1):1–26. [PubMed: 15109205]
12. Hunter P, Coveney PV, de Bono B, Diaz V, Fenner J, Frangi AF, Harris P, Hose R, Kohl P, Lawford P, McCormack K, Mendes M, Omholt S, Quateroni A, Skar J, Tegner J, Thomas SR, Tollis I, Tsamardinos I, van Beek JHGM, Viceconti M. A vision and strategy for the virtual physiological human in 2010 and beyond. *Phil Trans R Soc A.* 2010; 368:2595–614. [PubMed: 20439264]
13. Hunter PJ, Robbins P, Noble D. The IUPS human physiome project. *Pflug Arch Eur J Phys.* 2002; 445(1):1–9.
14. Hunter PJ, Smith NP, Fernandez J, Tawhai MH. Integration from proteins to organs: the IUPS Physiome Project. *Mech Ageing Dev.* 2005; 126(1):187–92. [PubMed: 15610778]
15. Weibel, ER. *Morphometry of the human lung.* Berlin: Springer-Verlag; 1963.
16. Horsfield K, Dart G, Olson DE, Filley GF, Cumming G. Models of the human bronchial tree. *J Appl Physiol.* 1971; 31:207–17. [PubMed: 5558242]
17. Glenny RW, Roberts TJ. Fractal properties of pulmonary blood flow: characterization of spatial heterogeneity. *J Appl Physiol.* 1990; 69(2):532–45. [PubMed: 2228863]
18. Glenny RW, Robertson HT. Fractal modeling of pulmonary blood flow heterogeneity. *J Appl Physiol.* 1991; 70(3):1024–30. [PubMed: 2032967]
19. Huang W, Tian Y, Gao J, Yen RT. Comparison of theory and experiment in pulsatile flow in cat lung. *Ann Biomed Eng.* 1998; 26:812–20. [PubMed: 9779954]
20. Lambert RK, Wilson TA, Hyatt RE, Rodarte JR. A computational model for expiratory flow. *J Appl Physiol.* 1982; 52:44–56. [PubMed: 7061277]
21. Venegas JG, Winkler T, Musch G, Vidal Melo MF, Layfield D, Tgavalekos N, Fischman AJ, Callahan RJ, Bellani G, Harris RS. Self-organized patchiness in asthma as a prelude to catastrophic shifts. *Nature.* 2005; 434:777–82. [PubMed: 15772676]
22. Wiggs BR, Moreno R, Hogg JC, Hilliam C. A model of the mechanics of airway narrowing. *J Appl Physiol.* 1990; 69(3):849–60. [PubMed: 2246172]
23. Hlastala MP, Glenny RW. Vascular structure determines pulmonary blood flow distribution. *News Physiol Sci.* 1999; 14:182–6. [PubMed: 11390848]
24. Fredberg JJ, Kamm RD. Stress transmission in the lung: pathways from organ to molecule. *Ann Rev Physiol.* 2006; 68:507–41. [PubMed: 16460282]
25. Griffith TM. Endothelial control of vascular tone by nitric oxide and gap junctions: a haemodynamic perspective. *Biorheology.* 2002; 39(3–4):307–18. [PubMed: 12122246]

26. Segars WP, Tsui B. MCAT to XCAT: The evolution of 4-D computerized phantoms for imaging research. *Proc IEEE*. 2009; 97(12):1954–68.
27. Eom J, Shi C, Xu XG, De S. Modeling respiratory motion for cancer radiation therapy based on patient-specific 4DCT data. *Med Image Comput Comput Assist Interv*. 2009; 12(Pt 2):348–55. [PubMed: 20426131]
28. Santhanam AP, Willoughby T, Shah A, Meeks S, Rolland JP, Kupelian P. Real-time simulation of 4D lung tumor radiotherapy using a breathing model. *Med Image Comput Comput Assist Interv*. 2008; 11(Pt 2):710–7. [PubMed: 18982667]
29. Werner R, Ehrhardt J, Schmidt R, Handels H. Patient-specific finite element modeling of respiratory lung motion using 4D CT image data. *Med Phys*. 2009; 36:1500–11. [PubMed: 19544766]
30. Bar-Yishay E, Hyatt RE, Rodarte JR. Effect of heart weight on distribution of lung surface pressures in vertical dogs. *J Appl Physiol*. 1986; 61(2):712–8. [PubMed: 3745065]
31. Matthews FL, West JB. Finite element displacement analysis of a lung. *J Biomech*. 1972; 5:591–600. [PubMed: 4665895]
32. West JB, Matthews FL. Stresses, strains, and surface pressures in the lung caused by its own weight. *J Appl Physiol*. 1972; 32(3):332–45. [PubMed: 5010043]
33. Tawhai MH, Hunter PJ, Tschirren J, Reinhardt JM, McLennan G, Hoffman EA. CT-based geometry analysis and finite element models of the human and ovine bronchial tree. *J Appl Physiol*. 2004; 97(6):2310–21. [PubMed: 15322064]
34. Bradley CP, Pullan AJ, Hunter PJ. Geometric modeling of the human torso using cubic Hermite elements. *Ann Biomed Eng*. 1997; 25:96–111. [PubMed: 9124743]
35. Fernandez JW, Mithraratne P, Thrupp SF, Tawhai MH, Hunter PJ. Anatomically based geometric modelling of the musculo-skeletal system and other organs. *Biomech Model Mechanobiol*. 2004; 2(3):139–55. [PubMed: 14685821]
36. Fernandez JW, Hunter PJ. An anatomically based patient-specific finite element model of patella articulation: towards a diagnostic tool. *Biomech Model Mechanobiol*. 2005; 4(1):20–38. [PubMed: 15959816]
37. Nowak N, Kakade PP, Annapragada AV. Computational fluid dynamics simulation of airflow and aerosol deposition in human lungs. *Ann Biomed Eng*. 2003; 31(4):374–90. [PubMed: 12723679]
38. Caro C. Swirling steady inspiratory flow in models of human bronchial airways (abstract from BMES annual meeting, RTP 2001). *Ann Biomed Eng*. 2001; 29(S1):S138.
39. Vial L, Perchet D, Fodil R, Caillibotte G, Fetita C, Prêteux F, Beigelman-Aubry C, Grenier P, Thiriet M, Isabey D, Sbirlea-Apiou G. Airflow modeling of steady inspiration in two realistic proximal airway trees reconstructed from human thoracic tomodensitometric images. *Comput Methods Biomech Biomed Engin*. 2005; 8(4):267–77. [PubMed: 16298849]
40. de Rochefort L, Vial L, Fodil R, Maître X, Louis B, Isabey D, Caillibotte G, Thiriet M, Bittoun J, Durand E, Sbirlea-Apiou G. In vitro validation of computational fluid dynamic simulation in human proximal airways with hyperpolarized ³He magnetic resonance phase-contrast velocimetry. *J Appl Physiol*. 2007; 102:2012–23. [PubMed: 17289906]
41. Choi LT, Tu JY, Li HF, Thien F. Flow and particle deposition patterns in a realistic human double bifurcation airway model. *Inhal Toxicol*. 2007; 19(2):117–31. [PubMed: 17169859]
42. Lin CL, Tawhai MH, McLennan G, Hoffman EA. Computational fluid dynamics multiscale simulation of gas flow in subject-specific models of the human lung. *IEEE Eng Med Biol*. 2009 May-Jun; 28(3):25–33.
43. Choi J, Tawhai MH, Hoffman EA, Lin CL. On intra- and intersubject variabilities of airflow in the human lungs. *Phys Fluids*. 2009 Oct.21(10):101901. (1994).
44. De Backer JW, Vos WG, Gorré CD, Germonpré P, Partoens B, Wuyts FL, Parizel PM, De Backer W. Flow analyses in the lower airways: patient-specific model and boundary conditions. *Med Eng Phys*. 2008; 30(7):872–9. [PubMed: 18096425]
45. Warren NJ, Crampin EJ, Tawhai MH. The role of airway epithelium in replenishment of evaporated airway surface liquid from the human conducting airways. *Ann Biomed Eng*. 2010 Dec; 38(12):3535–49. [PubMed: 20596780]

46. Kitaoka H, Takaki R, Suki B. A three-dimensional model of the human airway tree. *J Appl Physiol.* 1999 Dec; 87(6):2207–17. [PubMed: 10601169]
47. Murray CD. The physiological principle of minimum work applied to the angle of branching of arteries. *J Gen Physiol.* 1926; 9:835–41. [PubMed: 19872299]
48. Tgavalekos NT, Venegas JG, Suki B, Lutchen KR. Relation between structure, function, and imaging in a three-dimensional model of the lung. *Ann Biomed Eng.* 2003; 31(4):363–73. [PubMed: 12723678]
49. Tawhai MH, Pullan AJ, Hunter PJ. Generation of an anatomically based three-dimensional model of the conducting airways. *Ann Biomed Eng.* 2000; 28(7):793–802. [PubMed: 11016416]
50. Wang CY, Bassingthwaight JB, Weissman LJ. Bifurcating distributive system using Monte Carlo method. *Math Comput Modell.* 1992; 16(3):91–8.
51. Nelson TR, Manchester DK. Modeling of lung morphogenesis using fractal geometries. *IEEE Trans Med Imaging.* 1988; 7(4):321–7. [PubMed: 18230485]
52. Horsfield K, Relea FG, Cumming G. Diameters, lengths, and branching ratios in the bronchial tree. *Respir Physiol.* 1976; 26(3):351–6. [PubMed: 951538]
53. Phalen RF, Yeh HC, Schum GM, Raabe OG. Application of an idealized model to morphometry of the mammalian tracheobronchial tree. *Anat Rec.* 1978; 190:167–76. [PubMed: 629400]
54. Raabe, OG.; Yeh, H-C.; Schum, GM.; Phalen, RF. Tracheobronchial geometry: human, dog, rat, hamster. Vol. LF-53. Albuquerque, NM: Lovelace Foundation for Medical Education and Research; 1976.
55. Yin YB, Choi JW, Hoffman EA, Tawhai MH, Lin CL. Simulation of pulmonary air flow with a subject-specific boundary condition. *J Biomech.* 2010 Aug 10; 43(11):2159–63. [PubMed: 20483412]
56. Elliot FM, Reid L. Some new facts about the pulmonary artery and its branching pattern. *Clin Radiol.* 1965; 16(3):193–8. [PubMed: 14324878]
57. Bunton D, MacDonald A, Brown T, Tracey A, McGrath J, Shaw A. 5-Hydroxytryptamine- and U46619-mediated vasoconstriction in bovine pulmonary conventional and supernumerary arteries: effect of endogenous nitric oxide. *Clin Sci.* 2000; 98:81–9. [PubMed: 10600662]
58. Haefeli-Bleuer B, Weibel ER. Morphometry of the human pulmonary acinus. *Anatom Record.* 1988; 220:401–14.
59. Sapoval B, Filoche M, Weibel ER. Smaller is better-but not too small: a physical scale for the design of the mammalian pulmonary acinus. *Proc Natl Acad Sci U S A.* 2002 Aug 6; 99(16): 10411–6. [PubMed: 12136124]
60. Tawhai MH, Hunter PJ. Characterising respiratory airway gas mixing using a lumped parameter model of the pulmonary acinus. *Respir Physiol.* 2001; 127:241–8. [PubMed: 11504593]
61. Verbanck S, Paiva M. Model simulations of gas mixing and ventilation distribution in the human lung. *J Appl Physiol.* 1990; 69(6):2269–79. [PubMed: 2077025]
62. Horsfield K. Morphometry of the small pulmonary arteries in man. *Circ Res.* 1978 May; 42:593–37. [PubMed: 639181]
63. Pump KK. The circulation in the peripheral parts of the human lung. *Chest.* 1966; 49(2):119–29.
64. Fung YC, Sobin SS. Theory of sheet flow in lung alveoli. *J Appl Physiol.* 1969; 26:472–88. [PubMed: 5775333]
65. Zhou Q, Gao J, Huang W, Yen M. Vascular impedance analysis in human pulmonary circulation. *Biomed Sci Instrum.* 2006; 42:470–5. [PubMed: 16817653]
66. Zhuang FY, Fung YC, Yen RT. Analysis of blood flow in cat's lung with detailed anatomical and elasticity data. *J Appl Physiol.* 1983; 55(4):1341–8. [PubMed: 6629968]
67. Clark AR, Burrowes KS, Tawhai MH. Contribution of serial and parallel micro-perfusion to spatial variability in pulmonary inter- and intra-acinar blood flow. *J Appl Physiol.* 2010; 108(5):1116–26. [PubMed: 20110543]
68. Wagner P, McRae J, Read J. Stratified distribution of blood flow in secondary lobule of the rat lung. *J Appl Physiol.* 1967; 22(6):1115–23. [PubMed: 6027058]
69. West JB, Maloney JE, Castle BL. Effect of stratified inequality of blood flow on gas exchange in liquid-filled lungs. *J Appl Physiol.* 1972; 32(3):357–61. [PubMed: 5010045]

70. Burrowes KS, Tawhai MH, Hunter PJ. Modeling RBC and neutrophil distribution through an anatomically based pulmonary capillary network. *Ann Biomed Eng.* 2004; 32(4):585–95. [PubMed: 15117032]
71. Huang Y, Doerschuk CM, Kamm RD. Computational modeling of RBC and neutrophil transit through the pulmonary capillaries. *J Appl Physiol.* 2001; 90(2):545–64. [PubMed: 11160053]
72. Dhadwal A, Wiggs B, Doerschuk C, Kamm R. Effects of anatomic variability on blood flow and pressure gradients in the pulmonary circulation. *J Appl Physiol.* 1997; 83(5):1711–20. [PubMed: 9375343]
73. Milic-Emili J, Henderson JAM, Dolovich MB, Trop D, Kaneko K. Regional distribution of inspired gas in the lung. *J Appl Physiol.* 1966; 21(3):749–59. [PubMed: 5912744]
74. Hajji MA, Wilson TA, Lai-Fook SJ. Improved measurements of shear modulus and pleural membrane tension of the lung. *J Appl Physiol.* 1979; 47:175–81. [PubMed: 468657]
75. Lai-Fook SJ, Hyatt RE. Effects of age on elastic moduli of human lungs. *J Appl Physiol.* 2000; 89:163–8. [PubMed: 10904048]
76. Stamenovic D, Yager D. Elastic properties of air- and liquid-filled lung parenchyma. *J Appl Physiol.* 1988; 65(6):2565–70. [PubMed: 3215857]
77. Bates JHT, Lutchen KR. The interface between measurement and modeling of peripheral lung mechanics. *Resp Physiol Neurobiol.* 2005; 148(1–2):153–64.
78. Al-Mayah A, Moseley J, Velec M, Brock KK. Sliding characteristic and material compressibility of human lung: parametric study and verification. *Med Phys.* 2009 Oct; 36(10):4625–33. [PubMed: 19928094]
79. Fung YC, Tong P, Patitucci P. Stress and strain in the lung. *J Eng Mech Div.* 1978; 104:201–23.
80. Bates JHT. The multiscale manifestations of airway smooth muscle contraction in the lung. *J Appl Physiol.* 2010; 109(2):269–70. [PubMed: 20507972]
81. Anafi RC, Wilson TA. Airway stability and heterogeneity in the constricted lung. *J Appl Physiol.* 2001; 91:1185–92. [PubMed: 11509514]
82. Affonce DA, Lutchen KR. New perspectives on the mechanical basis for airway hyperreactivity and airway hypersensitivity in asthma. *J Appl Physiol.* 2006; 101(6):1710–9. [PubMed: 16902064]
83. Amin S, Majumdar A, Frey U, Suki B. Modeling the dynamics of airway constriction: effects of agonist transport and binding. *J Appl Physiol.* 2010; 109(2):553. [PubMed: 20507971]
84. Politi AZ, Donovan GM, Tawhai MH, Sanderson MJ, Bates JHT, Lauzon A-M, Sneyd J. A multiscale, spatially distributed model of asthmatic airway hyper-responsiveness. *J Theor Biol.* 2010; 266(4):614–24. [PubMed: 20678506]
85. Huxley A. Muscle structure and theories of contraction. *Prog Biophys Biophys Chem.* 1957; 7:255–318. [PubMed: 13485191]
86. Wang I, Politi AZ, Tania N, Bai Y, Sanderson MJ, Sneyd J. A mathematical model of airway and pulmonary arteriole smooth muscle. *Biophys J.* 2008; 94(6):2053–64. [PubMed: 18065464]
87. Hai C, Murphy R. Cross-bridge phosphorylation and regulation of latch state in smooth muscle. *Am J Physiol Cell Physiol.* 1988; 254(1):C99.
88. Fredberg J, Inouye D, Mijailovich S, Butler J. Perturbed equilibrium of myosin binding in airway smooth muscle and its implications in bronchospasm. *Am J Respir Crit Care Med.* 1999; 159(3):959–67. [PubMed: 10051279]
89. Burrowes KS, Hoffman EA, Tawhai MH. Species-specific pulmonary arterial asymmetry determines species differences in regional pulmonary perfusion. *Ann Biomed Eng.* 2009; 37(12):2497–509. [PubMed: 19768544]
90. Glenny RW. Counterpoint: Gravity is not the major factor determining the distribution of blood flow in the healthy human lung. *J Appl Physiol.* 2008; 104(5):1533–5. [PubMed: 18450991]
91. Glenny RW, Bernard S, Robertson HT, Hlastala MP. Gravity is an important but secondary determinant of regional pulmonary blood flow in upright primates. *J Appl Physiol.* 1999; 86(2):623–32. [PubMed: 9931200]
92. Glenny RW, Lamm WJE, Albert RK, Robertson HT. Gravity is a minor determinant of pulmonary blood flow distribution. *J Appl Physiol.* 1991; 71:620–9. [PubMed: 1938736]

93. Clark AR, Tawhai MH, Hoffman EA, Burrowes KS. The interdependent contributions of gravitational and structural features to perfusion distribution in a multi-scale model of the pulmonary circulation. *J Appl Physiol.* 2011; 110(4):943–55. [PubMed: 21292845]

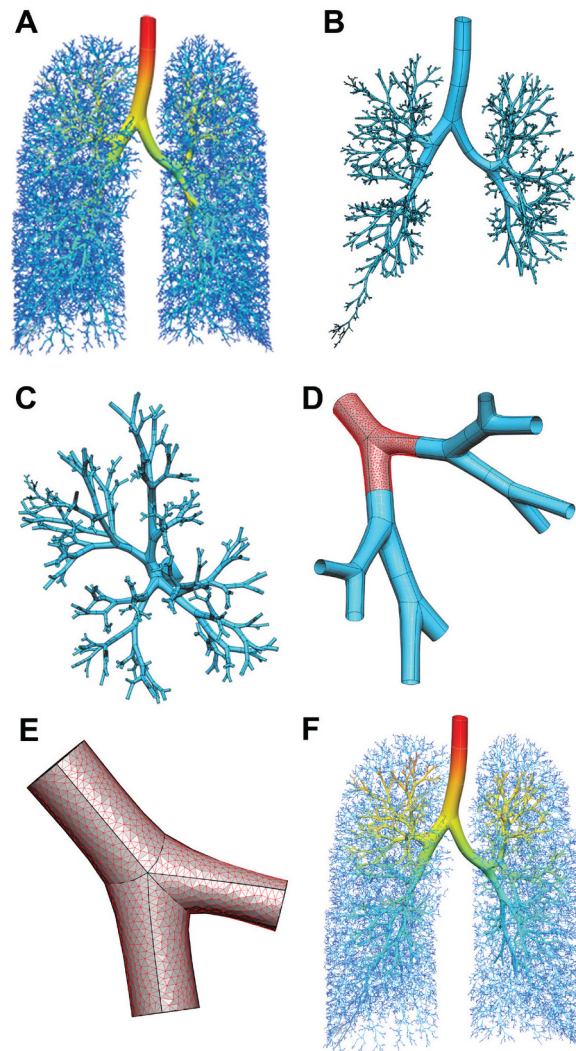


FIGURE 1. Generation of a 3D-1D coupled model for the human airway tree geometry: (A) a 1D (centerline) airway mesh, rendered with cylinders to illustrate the size of the airway radii; (B) 2D surface geometry generated over a selected portion of the 1D tree; (C,D,E) successive zooming to a subset of the airways in (B), illustrating the unstructured mesh (in red and gray) that is generated within the curvilinear high-order surface mesh (in blue); (F) combined CFD-ready mesh and 1D airways (lines) (figure adapted with permission from Lin et al.⁹).

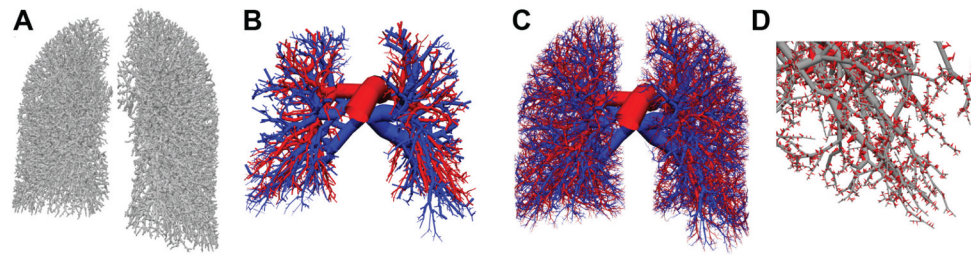


FIGURE 2.

Generation of an anatomically based model for the extra-acinar vessels of the pulmonary circulation: (A) rendered isosurfaces of vessels segmented from multidetector row computed tomography (MDCT) data from the Human Lung Atlas; (B) MDCT-derived arterial (red) and venous (blue) vessels; (C) includes vessels generated into the lobar volume using the volume-filling branch (VFB) algorithm; (D) close-in view of supernumerary vessels (red) with accompanying vessels (gray) (from Burrowes et al.,⁵ *Journal of Applied Physiology*, 2005, American Physiological Society, used with permission).

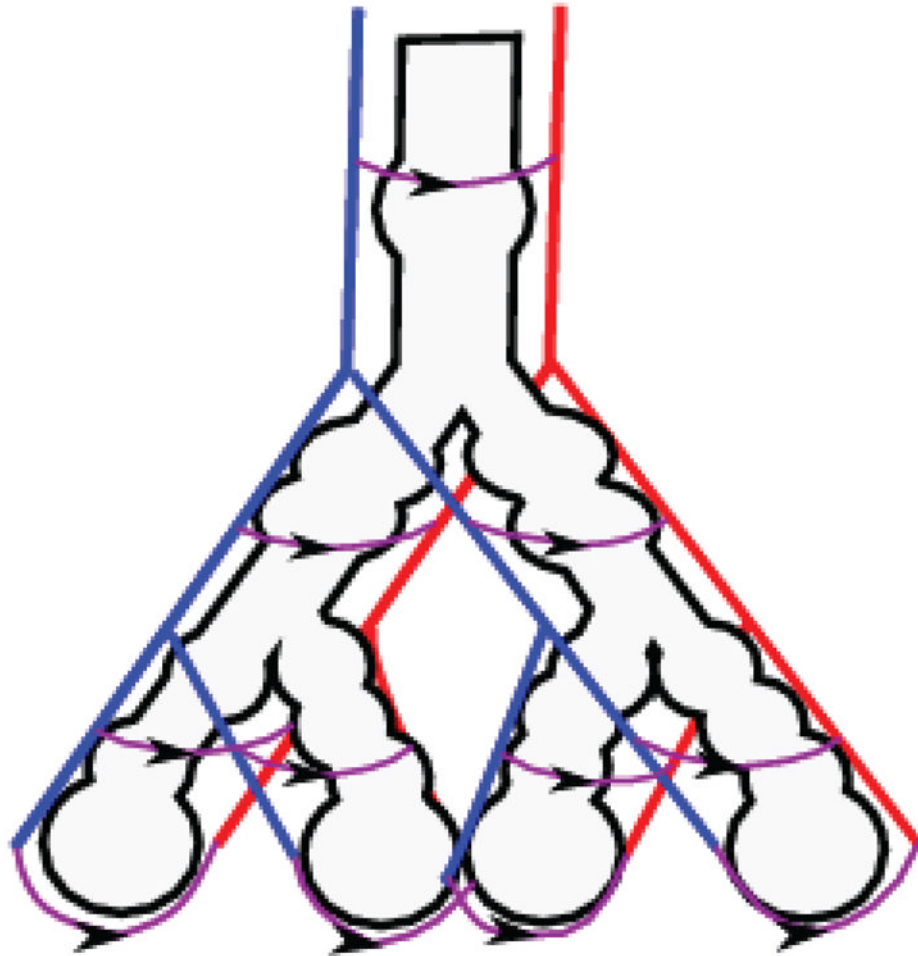


FIGURE 3. The ladderlike acinar structure modeled by Clark et al.⁶⁷; arterioles (blue) and venules (red) were modeled as distinct elastic vessels with capillary sheets (purple with arrows in the direction of blood flow) connecting them at each acinar airway generation (from Clark et al.,⁶⁷ *Journal of Applied Physiology*, 2010, American Physiological Society, used with permission).

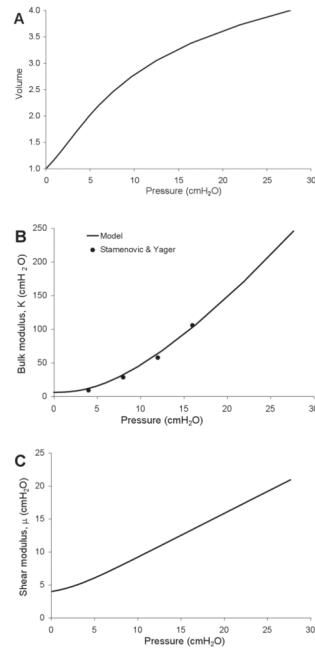


FIGURE 4. Stress-strain behavior of the strain energy density function employed by Tawhai et al.¹⁰ to predict lung tissue displacement due to gravity: (A) pressure-volume relationship; (B and C) effective bulk and shear moduli, respectively, calculated from the continuum model at increasing inflation pressures (from Tawhai et al.,¹⁰ *Journal of Applied Physiology*, 2009, American Physiological Society, used with permission).

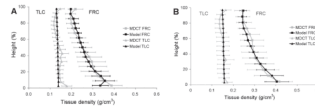


FIGURE 5.

Tissue density distribution predicted in the supine posture using a continuum model for finite deformation elasticity. Results illustrate mean tissue density calculated within 10 mm wide slices of lung or model, with the slices oriented perpendicular to the direction of gravity (gravity and y-axis are oriented posterior-anterior). The error bars shown \pm SD for the density in each slice. Model results (black) are compared with tissue density calculated from CT imaging (gray) in two disparate subjects: (A) healthy male; (B) female with small airways disease (from Tawhai et al.,¹⁰ *Journal of Applied Physiology*, 2009, American Physiological Society, used with permission).

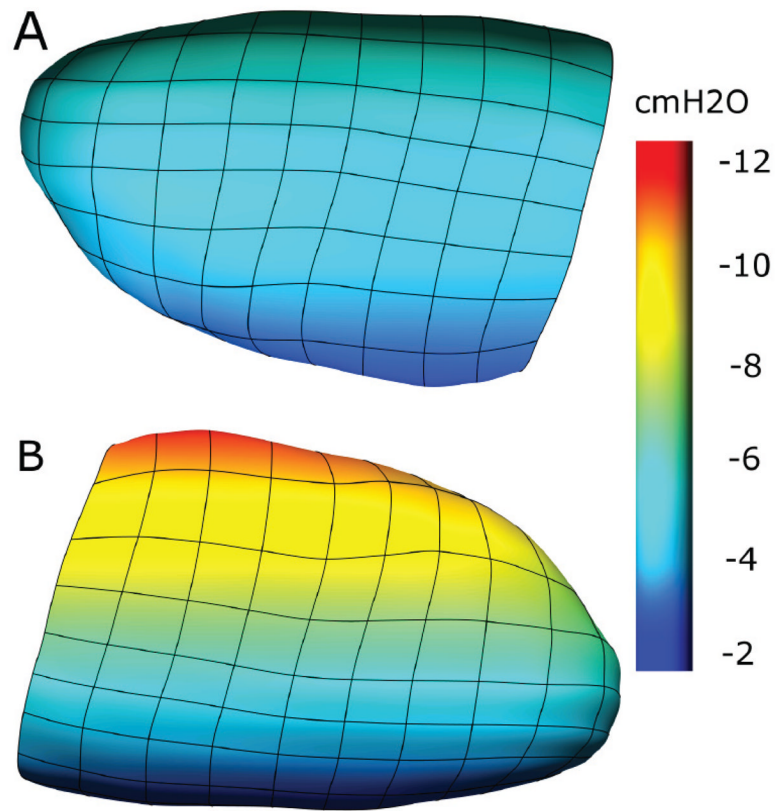


FIGURE 6. Surface (pleural) pressures predicted for one subject, using a continuum model for tissue deformation under the action of gravity and the weight of the lung: (A) shows surface pressures in the prone model, which has a smaller predicted deformation gradient and hence pleural pressure gradient than that predicted for the supine lung in (B) (from Tawhai et al.,¹⁰ *Journal of Applied Physiology*, 2009, American Physiological Society, used with permission).

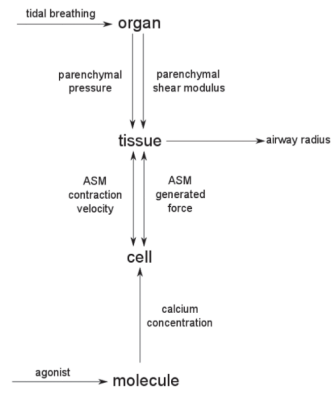


FIGURE 7.

A schematic representation of ASM force generation; ASM force is opposed by parenchymal tethering and airway wall mechanics, and these forces must be balanced in order to determine the airway radius; this process is repeated for each airway at each time step.

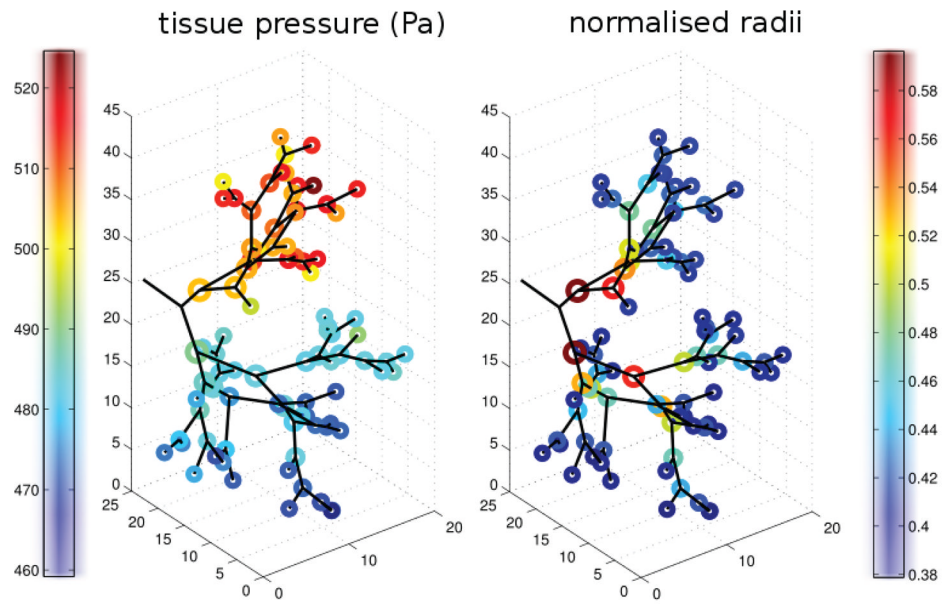


FIGURE 8. Emergent spatial heterogeneity in the distributions of pressure (left panel) and airway radius (right panel) at the conclusion of a simulated agonist challenge (results are reproduced from Politi et al.⁸⁴ with permission from Elsevier).